Improved Satellite Launcher Navigation Performance by Using the Reference Trajectory Data

Yanick Beaudoin[1], André Desbiens[1], Eric Gagnon[2], and René Jr. Landry[3]

[1]Université Laval
[2]Defence Research and Development Canada
[3]École de technologie supérieure de Montréal
Email: yanick.beaudoin.1@ulaval.ca

The navigation is a critical element of a satellite launcher. The objective of this research is to evaluate the additional precision and robustness provided to the navigation solution by using the reference trajectory data. To include this information, the error state model of a GPS/INS configuration is augmented to estimate the difference between the launcher and the reference trajectory attitude data. The assessment of the precision gain is made using the standard deviation of the attitude, velocity and position estimation errors. The robustness is evaluated considering the loss of precision caused by a GPS outage. The velocity estimation is slightly improved, but the attitude estimation greatly benefits from the additional information. Also, the robustness to a GPS outage is greatly improved for all estimated values. The augmented model can withstand errors in the variances of the external perturbations. However, this one could be sensitive to modelling errors.

KEY WORDS

Satellite Launcher Navigation, Reference Trajectory, Data Fusion

1. INTRODUCTION. The navigation is a critical element of a satellite launcher. In order to be able to correct its trajectory properly, it is important to know the position, velocity and attitude of the launcher with the best possible accuracy. For an equivalent accuracy and robustness, the price of the navigation solution does not change depending on the size of the launcher. So, on a small launcher targeting a low orbit, it may take a significant proportion (Barbour, 2011; Schmidt, 2010; Koelle, 2005). Therefore, it is advantageous to use "free" sources of information that require no sensor.

To increase accuracy and robustness of navigation solutions, the common approaches are developing more efficient sensors (Samaan and Theil, 2011; Yu et al., 2010; Brown and Mathews, 2007; Titterton and Weston, 2004), exploiting the redundancy of sensors (Yuksel et al., 2010; Tanenhaus et al., 2010; Bancroft, 2009; Giroux, 2004), combining multiple sensors with complementary qualities (Zhang et al., 2011; Hao et al., 2010; Ali and Fang, 2009; Theil et al., 2009; Ning and Fang, 2008; Theil et al., 2008; Sedlak, 1997; Kachmar and Wood, 1995) or employing more efficient fusion algorithms than the extended Kalman filter (Gross et al., 2010;

Ali and Fang, 2009; Wang et al., 2008; Ali and Jiancheng, 2006; Groves and Long, 2005). Nevertheless, none of the solutions exploits the fact that the optimal trajectory that should be followed by the vehicle is calculated before the launch. The Ariane 5 navigation exploits a ballistic trajectory during the coast phase, which begins around an altitude of 1000 km and can last up to 5 hours. This approach is less sensitive to estimation drift than the INS (Inertial Navigation System) used during the powered phase (Belin et al., 2010). However, these two approaches are employed independently depending on the flight phase.

Most vehicles follow a different path for each use and this one can be severely disrupted along the way or simply be unknown. One only has to think of a Sunday car ride. However, the economic imperatives of launching a satellite involve trajectory optimization to minimize the cost. In addition, the sources of disturbance are mainly concentrated in the endoatmospheric flight phase, which is relatively short (Vachon, 2012; Belin et al., 2010; Vachon et al., 2010). Therefore, the real trajectory of the launcher should be very close to the reference trajectory. This knowledge adds a source of navigational information without requiring additional sensors.

The main idea is that initially, the position and attitude of the launcher are well known. As the mission progresses, the vehicle may deviate from the reference trajectory because of the disturbances. By weighting the confidence we have on the fact that the launcher follows the reference trajectory, it is possible to exploit this information to improve the performance of the navigation solution.

The GNC (Guidance, Navigation and Control) system is the most important investment in development, testing and validation with respect to software design (Ferguson, 2011). To avoid having to repeat the certification of equipment already present and which have been proven, it may be desirable to avoid the modification of existing systems (Ferguson, 2011; Goodman and Propst, 2008). The use of the reference trajectory data requires no changes in the guidance and control equipment because, for the implementation considered, the data is stored in the memory of the navigation solution.

During the endoatmospheric phase, open loop guidance is performed and only the attitude of the vehicle is controlled. Therefore, the effect of external disturbances on the position of the launcher should be compensated in the exoatmospheric phase (Vachon, 2012; Lu et al., 2003; Hanson et al., 1995). Considering the differences between these two phases, they are treated independently. Thus, this article aims to validate the concept of using data from the reference trajectory in a navigation solution for the endoatmospheric phase. The exoatmospheric phase will be discussed in a later paper. The second section introduces the GNC function principle. The third section presents the simplified model employed to validate the concept proposed. The fourth section shows the mathematical development of the resulting navigation solution. The fifth section compares the new navigation solution, which uses the reference path, to a solution that does not use it.

2. GNC FUNCTION. The GNC function manages the movement of the launcher through-out the mission. The process consists of two nested loops. The outer loop establishes the optimal trajectory to be followed by the launcher to achieve the objective of the mission and the inner loop takes the actions to match the optimal trajectory (Vachon, 2012; Bletsos, 2004; de Castro Leite Filho, 2000). Also, the GNC function has access to *a priori* knowledge. Data includes information on wind profiles, on the vibrational patterns, on the desired orbit and on the reference path (Vachon, 2012; Bletsos, 2004; Lu et al., 2003; Hanson et al., 1995).

3. SIMPLIFIED MODEL. A complete non linear simulator of the launcher is available. However, in order to prove the concept and make the analysis clearer, a simplified model is

exploited in the course of this paper. This one considers the control and launcher grouped as shown in figure 1, where a_{ref}^B and $[\omega_{ref}]_{IB}^B$ are respectively the reference acceleration and angular velocity expressed in the body frame. These values will be used as the unperturbed forces acting on the launcher. $[\omega_w]_{IB}^B$ is the angular velocity induced by the wind represented in the body frame. r_{ref}^E is the reference position given in the Earth frame, r_e^E and v_e^E are the estimated position and velocity expressed in the Earth frame. $[\mathbf{T_{ref}}]_\mathbf{B}^\mathbf{E}$, $[\mathbf{T_d}]_\mathbf{B}^\mathbf{E}$ and $[\mathbf{T_e}]_\mathbf{B}^\mathbf{E}$ are rotation matrices from the body frame to the Earth frame representing respectively the reference, desired and estimated attitudes. a_r^B, $[\omega_r]_{IB}^B$, v_r^E and r_r^E are the real acceleration, angular velocity, velocity and position of the launcher, δa_m^B, $[\delta\omega_m]_{IB}^B$, δv_m^E and δr_m^E are the corresponding measurements and δa_m^B, $[\delta\omega_m]_{IB}^B$, δv_m^E and δr_m^E the associated measurement noises. The INS values (accelerometers and rate gyroscopes) are represented in the body frame and the GPS (Global Positioning system) values (position and velocity) are in the Earth frame. To ensure an easy transfer of the navigation algorithm to the nonlinear simulator, the simplified model is designed to be as close as possible to this one.
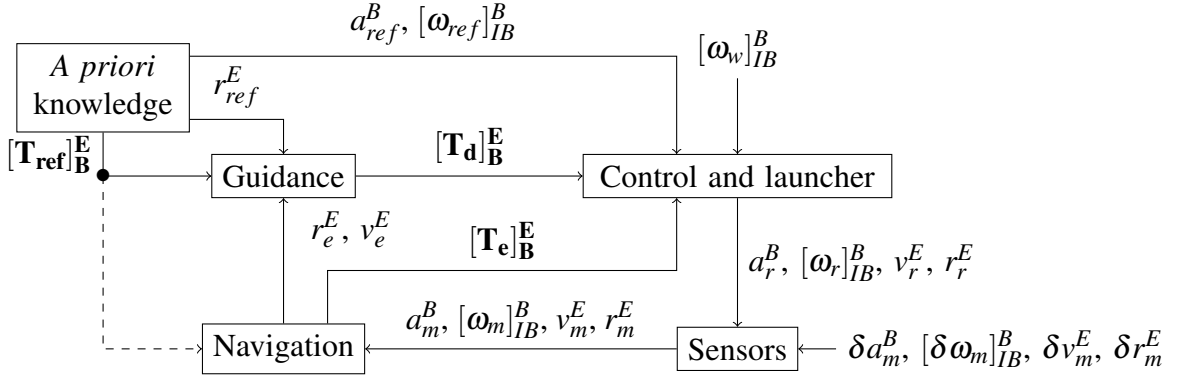

Figure 1: Simplified GNC loops. The dashed line represents the reference attitude data added to the navigation

The gain scheduling performed in the control function to account for the change in the dynamics of the launcher tends to makes the overall control and launcher angular dynamics equation constant. Therefore, for the purposes of this work, a linear time invariant function will be exploited. Since open loop guidance is performed during the endoatmospheric phase, the desired attitude sent to the control function corresponds to the reference trajectory attitude $[\mathbf{T_d}]_\mathbf{B}^\mathbf{E} = [\mathbf{T_{ref}}]_\mathbf{B}^\mathbf{E}$. As mentioned previously, the vehicle position and velocity are not controlled, therefore only the attitude data from the reference trajectory is used as additional information for the navigation.

For the rest of the analysis, the guidance, the control and the launcher are considered ideal, unless otherwise stated. Thus, their model is identical to the reality. The reference trajectory takes into account the wind profile on the launch site and it can be updated using the day of launch wind data. But, even with this information, the stochastic nature of the wind makes it the most difficult perturbation to anticipate (Duplain, 2012; Lu et al., 2003; Mori, 1999; Hanson et al., 1995). Therefore, this one is the only external disturbance considered in the analysis presented. Accordingly, in the course of this article, the only sources of errors making the launcher diverging from its reference trajectory are the navigation error and the wind.

To further simplify the model some assumption are made:

- A null wind is used as the wind profile.
- The launcher is rigid.

- The actual wind is modeled by an angular velocity perturbation.
- The Earth is considered to be spherical for gravity calculations.
- The sideslip angle is considered small enough to neglect its effect on the aerodynamic force.
- Except for the wind, the effect of the forces affecting the axial acceleration and the angular velocity is precomputed.
- The roll rate is considered as unaffected by the wind.
- Only the random walk is modeled for the accelerometers and rate gyroscopes imperfections (i.e. the bias is known and canceled, and the mission is short enough to consider it to be constant).

These simplifications are intended to avoid overburdening the analysis and do not have impact on the understanding of the principle. For the purpose of this research, the endoatmospheric phase ends when the guidance switches from open loop to close loop mode. This occurs 160 seconds after the beginning of the mission. At this point the altitude is around 100km which corresponds to the Kármán line.

4. MATHEMATICAL DEVELOPPEMENT OF THE NAVIGATION SOLUTION. This section presents the mathematical development of a navigation solution which uses the reference trajectory. First, the propagation of the divergence between the actual and the reference attitude is analysed for the yaw angle. Then, the implementation of the principle in a three-dimension navigation solution is introduced.

4.1. *Propagation Of The Divergence From The Reference Attitude.* In order to exploit the reference trajectory in the navigation solution, it is important to understand how the difference between the actual path of the vehicle and the reference trajectory propagates. As previously mentioned, during the endoatmospheric phase, only the attitude data from the reference trajectory is employed. Figure 1 is used to better understand the mathematical developments presented in this section.

The development in this section is done in the body frame; this allows to demonstrate the principle considering only one dimension. As the principle is the same for each axis, only the propagation of yaw is presented here.

The open loop transfer function for the control and launcher yaw dynamics is $G_\psi(s)$. Considering that wind effect is represented by angular velocity variation, this one must be integrated to get angular deviation, so let's define:

$$G_I(s) = \frac{1}{s} \tag{1}$$

The real yaw ψ_r of the launcher is given by:

$$\psi_r = G_\psi(s)\left(\psi_d - \psi_e\right) + G_I(s)\omega_{w\psi} \tag{2}$$

where $\omega_{w\psi}$ is the yaw angular speed induced by the wind, ψ_d and ψ_e are respectively the desired and estimated yaw. The equation of the latter is:

$$\psi_e = \psi_r + \delta\psi_e \tag{3}$$

where $\delta\psi_e$ is the yaw estimation error of the navigation. Inserting (3) in (2):

$$\psi_r = G_\psi(s)\left(\psi_d - \psi_r - \delta\psi_e\right) + G_I(s)\omega_{w\psi} \tag{4}$$

and isolating ψ_r in the previous equation gives:

$$\psi_r = \underbrace{\frac{G_\psi(s)}{1 + G_\psi(s)} \psi_d}_{\substack{\text{unperturbated} \\ \text{trajectory}}}$$

$$+ \underbrace{\frac{G_I(s)}{1 + G_\psi(s)} \omega_{w\psi}}_{\substack{\text{error caused by} \\ \text{the wind}}} - \underbrace{\frac{G_\psi(s)}{1 + G_\psi(s)} \delta\psi_e}_{\substack{\text{error caused by} \\ \text{the navigation}}} \tag{5}$$

The reference yaw ψ_{ref} is the yaw which would be followed without perturbations, thus it can be expressed as only the first term of equation (5):

$$\psi_{ref} = \frac{G_\psi(s)}{1 + G_\psi(s)} \psi_d \tag{6}$$

Therefore, the divergence of the launcher from the reference attitude is given by:

$$\delta\psi_{ref} = \psi_r - \psi_{ref} \tag{7}$$

$$= \frac{G_I(s)}{1 + G_\psi(s)} \omega_{w\psi} - \frac{G_\psi(s)}{1 + G_\psi(s)} \delta\psi_e \tag{8}$$

Unfortunately, for the observation equation, ψ_r and $\delta\psi_{ref}$ are unknown values. Inserting (3) in (7) gives:

$$\delta\psi_{ref} = \psi_e - \delta\psi_e - \psi_{ref} \tag{9}$$

$$\psi_e - \psi_{ref} = \delta\psi_{ref} + \delta\psi_e \tag{10}$$

$$\Delta\psi_{ref} = \delta\psi_{ref} + \delta\psi_e \tag{11}$$

where $\Delta\psi_{ref}$ is the difference between the estimated and reference yaw, which is a known value.

4.2. *Implementation.* The baseline navigation system uses a GPS/INS in a loosely coupled configuration. The error state model estimates the attitude, velocity and position errors in the Earth frame (Ma et al., 2009; Savage, 2007; Waldmann, 2007). This model is augmented to estimate the difference between the launcher and reference attitude. Since the launcher attitude dynamics equation is given in the body frame, the error state vector of the augmented model is also defined in the body frame. The complete error state model is given by:

$$\begin{bmatrix} \dot{x}_{lc}^E \\ \dot{x}_a^B \end{bmatrix} = \begin{bmatrix} A1 & 0 \\ A2 & A3 \end{bmatrix} \begin{bmatrix} x_{lc}^E \\ x_a^B \end{bmatrix}$$

$$+ \begin{bmatrix} B1 & B2 & 0 \\ 0 & 0 & B3 \end{bmatrix} \begin{bmatrix} [\delta\omega_m]_{IB}^B \\ \delta a_m^B \\ [\omega_w]_{IB}^B \end{bmatrix} \tag{12}$$

$$\begin{bmatrix} \delta v_e^E \\ \delta r_e^E \\ \Delta\Psi_{ref}^E \end{bmatrix} = \begin{bmatrix} C1 & 0 \\ C2 & 0 \\ C3 & C4 \end{bmatrix} \begin{bmatrix} x_{lc}^E \\ x_a^B \end{bmatrix} \tag{13}$$

5

where x_{lc}^E is the loosely coupled error state vector, $A1$ is the corresponding propagation matrix, $B1$ and $B2$ are the rate gyroscope and accelerometers noise input matrices. $[\delta\omega_m]_{IB}^B$ and δa_m^B are the rate gyroscope and accelerometers noise vectors given in the body frame. $C1$ and $C2$ are the observation matrices for the velocity error δv_e^E and the position error δr_e^E. The details of these vectors and matrices can be found in appendix.

The vector x_a^B represents the state that estimates the difference between the launcher and reference attitude. The matrix $A3$ represents the close loop angular dynamics of the launcher. $A2$ indicates the propagation of the loosely coupled attitude error into the augmented model (i.e. how the attitude estimation error of the navigation is manifested in the launcher angular dynamics). $B3$ is the wind effect input matrix and $[\omega_w]_{IB}^B$ is the angular velocity created by the wind. Finally, $C3$ and $C4$ combine the loosely coupled attitude estimation error and the difference between the launcher and reference attitude to compute the difference between the navigation and reference attitude $\Delta\Psi_{ref}^E$. The sizes and values of these matrices and vectors depend on the angular dynamics of the launcher, the details for those used in the current works can be found in appendix.

5. PERFORMANCE COMPARISON. The performance is analysed for four conditions. The first two are intended to validate the principle of using the reference trajectory. For those tests, the navigation model corresponds exactly to the launcher model, The precision gain and the robustness to GPS outage are evaluated using the estimation covariance matrix of the navigation Kalman filter. However, in real life, the launcher model and the statistics of the perturbations affecting it are not always perfectly known. For this reason, two basic robustness tests are performed on the augmented model to ensure that this one can handle both modelling and parameters errors. First, the simulation parameters are presented, then the simulation results are analysed.

5.1. *Simulation Parameters.* The simulated mission is intended to put a satellite on a circular sun-synchronous orbit at an altitude of 500 km. The launch is performed from Churchill, Manitoba in Canada. Figure 2(a) shows the launch site and figure 2(b) the trajectory as a function of time during the endoatmospheric phase. During this phase, two engines are fired. One during the first 109 seconds and the second for the remaining time.

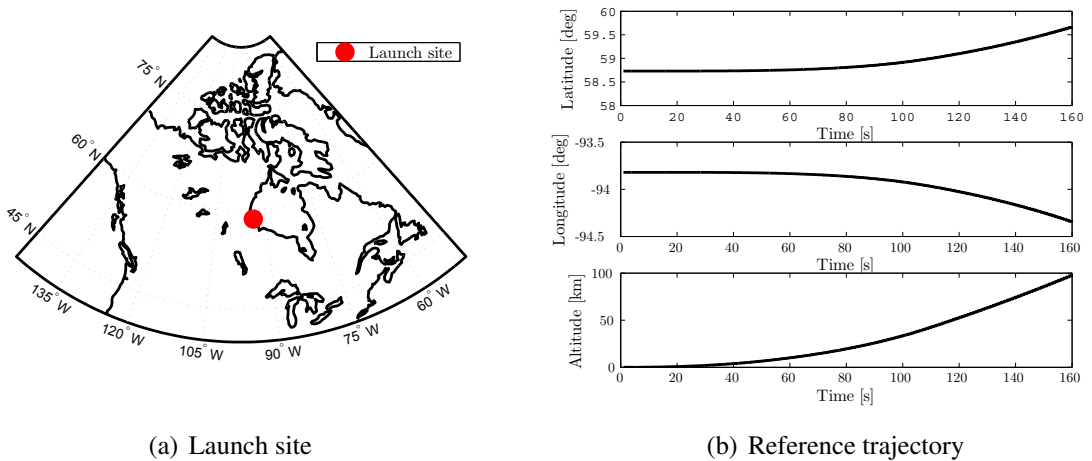

(a) Launch site

(b) Reference trajectory

Figure 2: Endoatmospheric phase details

Based on previous works achieved on the non linear launcher simulator, wind effect becomes negligible after 90 seconds of flight where the altitude is 26 km. Considering this, the

simulations are done with a high wind power for the first 90 seconds of the mission and negligible wind power afterwards. In order to evaluate the robustness of the navigation solution to a GPS outage, the whole endoatmospheric phase is performed without GPS measurement. This one is simulated by a very high noise level on the velocity and position measurements. The following list summarizes the simulation parameters:

- Variance of the angular velocity introduced by the wind:
  - during the first 90 seconds of flight: $1 \times 10^{-4} (rad/s^2)^2$
  - from 90 to 160 seconds of flight: $1 \times 10^{-10} (rad/s^2)^2$
- Sensors noise (tactical grade):
  - rate gyroscope random walk: $5°/h/\sqrt{Hz}$
  - accelerometer random walk: $400\mu g/\sqrt{Hz}$
- Variance of GPS measurement noise (with GPS signal):
  - velocity: $0.1 (m/s)^2$
  - position: $10 m^2$
- Variance of GPS measurement noise (without GPS signal):
  - velocity: $1 \times 10^8 (m/s)^2$
  - position: $1 \times 10^{10} m^2$

The dynamics of the launcher and control equations are based on previous work accomplished on the non linear launcher simulator (Duplain, 2012). The transfer function for the open loop yaw dynamics is given by:

$$G_\psi(s) = \frac{-0.57(4s+1)(9.25s+1)}{4s^2(-1.22s+1)(0.144s+1)} \tag{14}$$

The same function is used for the open loop pitch dynamics:

$$G_\theta(s) = G_\psi(s) \tag{15}$$

The open loop roll dynamics is:

$$G_\phi(s) = \frac{1.2}{s(2s+1)} \tag{16}$$

The state covariance matrix of the Kalman filter is calculated based on the input and model noises (modelling errors, limited mathematical precision, etc.). Since the latter is unknown, some tests were performed in order to tune the Kalman filter state covariance matrix. The tuning is done to accommodate many sensor precision and wind levels. Therefore, it is not specifically tuned for the tested configurations.

The performance analysis is realized on two models. The first one is using a loosely coupled GPS/INS and is the baseline. The other one adds the reference trajectory to the baseline model and is called the augmented model.

Finally, the robustness to parameters and modelling error are studied using a Monte-Carlo simulation composed of 56 launches. The real standard deviations are calculated from the Monte-Carlo simulation. The navigation Kalman filter provides the estimated standard deviations through the estimation covariance matrix. The robustness to parameters error is evaluated by underestimating the wind perturbation variance by a factor of 10 in the navigation algorithm. The robustness to modelling error is verified by doubling the gain of the three open loop angular dynamics equations in the error state model of the navigation.

5.2. *Results.* In order to make the analysis more understable, all results are represented in the body frame. Figures 3, 4 and 5 show the results obtained when the GPS signal is present. Considering the great precision already achieved with the baseline model and the fact that this part of the flight is greatly affected by the wind, the gain expected with the addition of the reference attitude was not high. Nevertheless, a great improvement is observed on the estimation of the roll and yaw as seen on figure 3. The considerable gain in the roll estimation can be explained by the fact that this one is unaffected by the wind. Also, the launcher acceleration is headed towards one direction, which makes the roll observability weak in the baseline model. Considering this, the GPS measurements can only barely improve the precision of the roll estimation obtained with the rate gyroscope. Even if the gain is less significant, the pitch estimation is also improved. Figure 4 shows a modest improvement on the velocity estimation and figure 5 shows that the position estimation do not benefits from the augmented model. But, the observability of these two values is good and they can be directly corrected using the GPS measurements, which limits the potential gain. However, some other tests were performed with different sensors grades and wind levels. The augmented model always outperforms the baseline model, or at least equals the results of this one. The weakest gains are obtained with very good sensors used in highly windy condition. In this case the improvement is almost null. As the sensors quality or the wind level is reduced, the precision gain becomes more evident. The precision improvements at the end of the endoatmospheric phase are summarized in table 1.
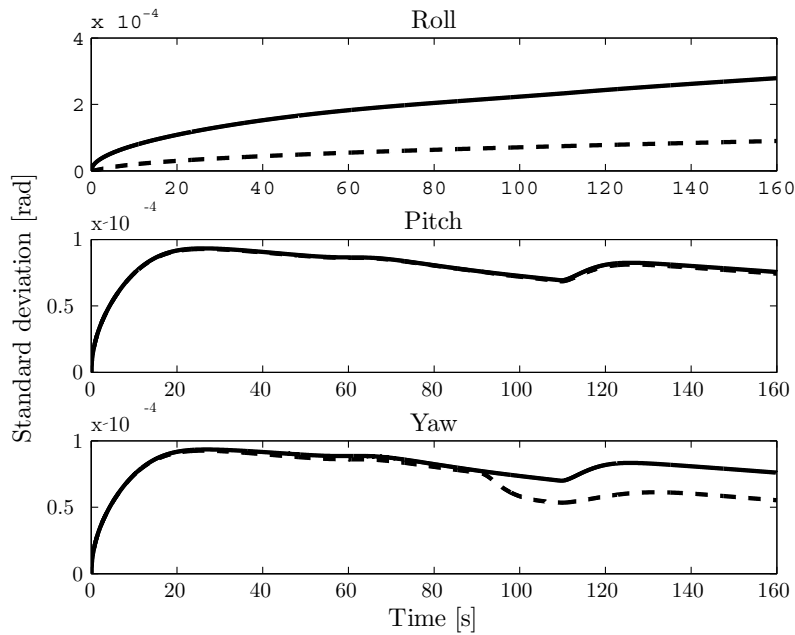

Figure 3: Attitude error standard deviations (with GPS). The solid line represents the baseline model and dashed line the augmented model.
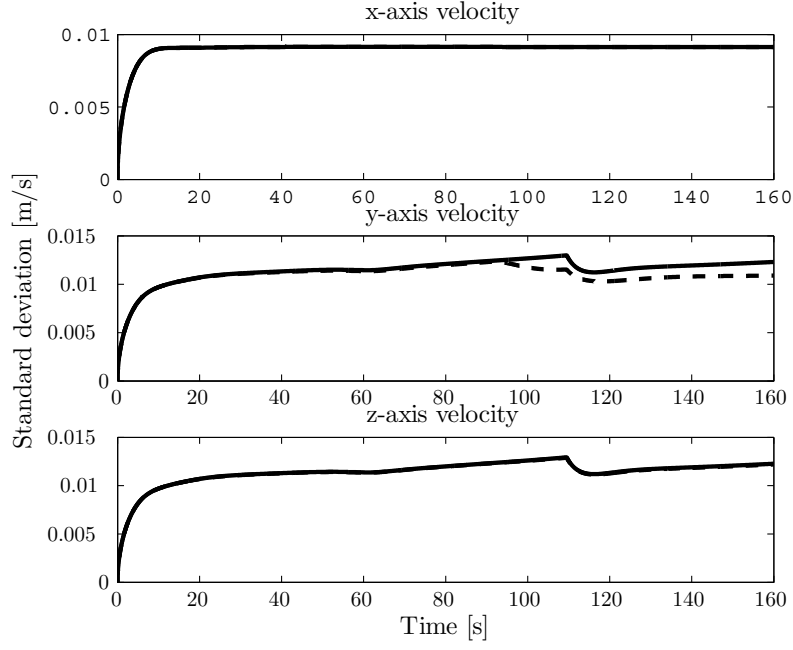
Figure 4: Velocity error standard deviations (with GPS). The solid line represents the baseline model and dashed line the augmented model.
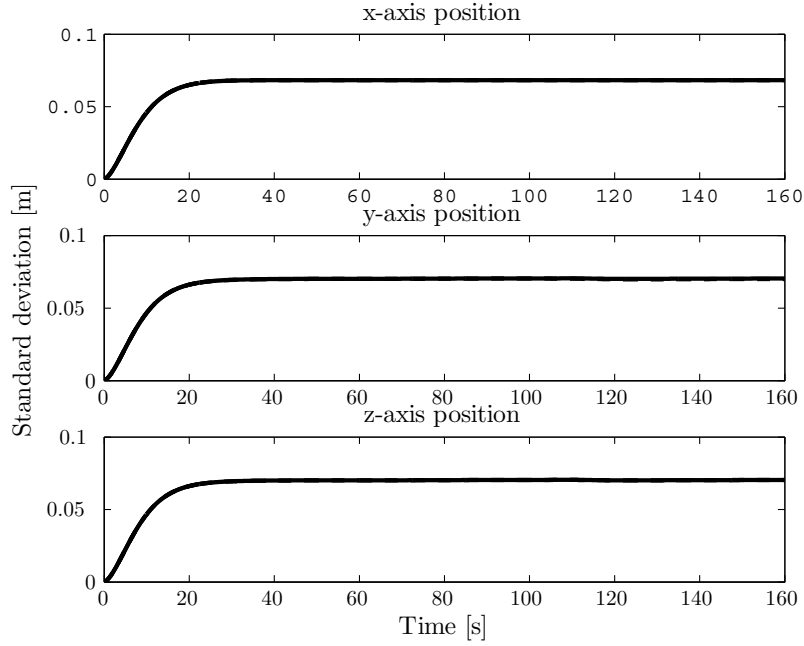

Figure 5: Position error standard deviations (with GPS). The solid line represents the baseline model and dashed line the augmented model.

Figures 6, 7 and 8 present the results without GPS signal. The first plot of figure 6 shows that the roll precision is almost the same as when GPS is present. This confirms that GPS is not of great assistance to estimate this angle. The improvement of pitch and yaw estimations is of the same order of magnitude as the one obtained without the GPS. In most INSs, it is the gyroscopes accuracy which is limiting the overall accuracy (Woodman, 2007). Therefore, even

if only the attitude data of the reference trajectory is exploited, a substantial gain in the velocity and position estimations precision is observed, as it is shown in figures 7 and 8. This makes evident that the attitude estimation precision has a big impact on the velocity and position estimations. Table 1 summarizes the gains obtained at the end of the endoatmospheric phase.
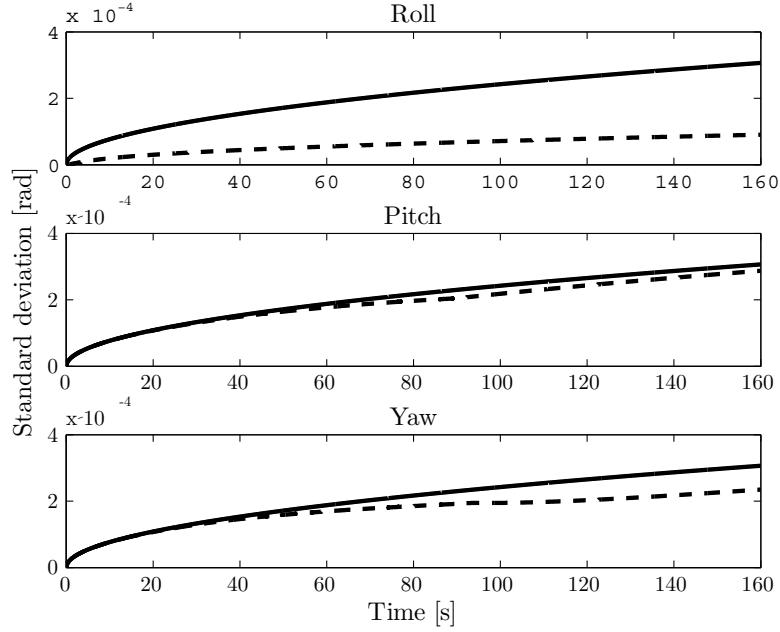

Figure 6: Attitude error standard deviations (without GPS). The solid line represents the baseline model and dashed line the augmented model.
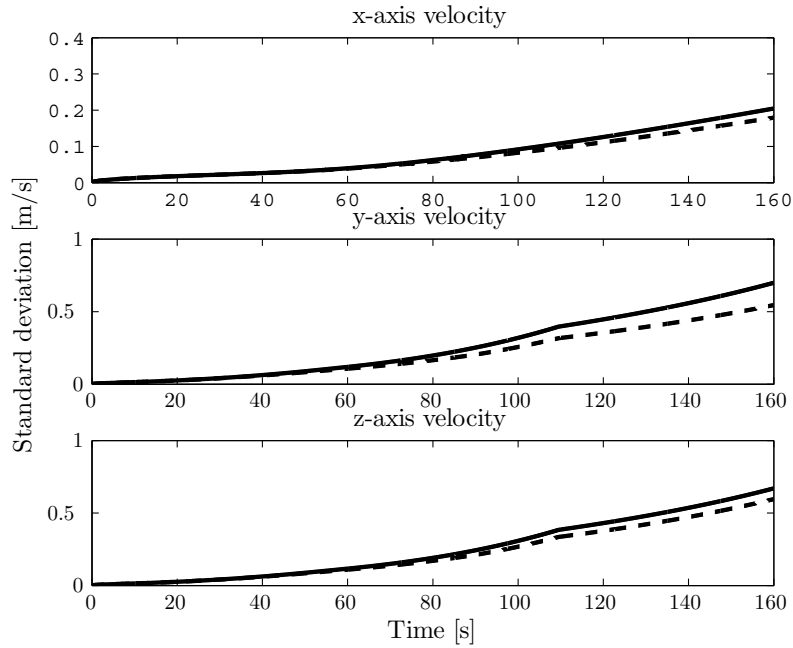

Figure 7: Velocity error standard deviations (without GPS). The solid line represents the baseline model and dashed line the augmented model.
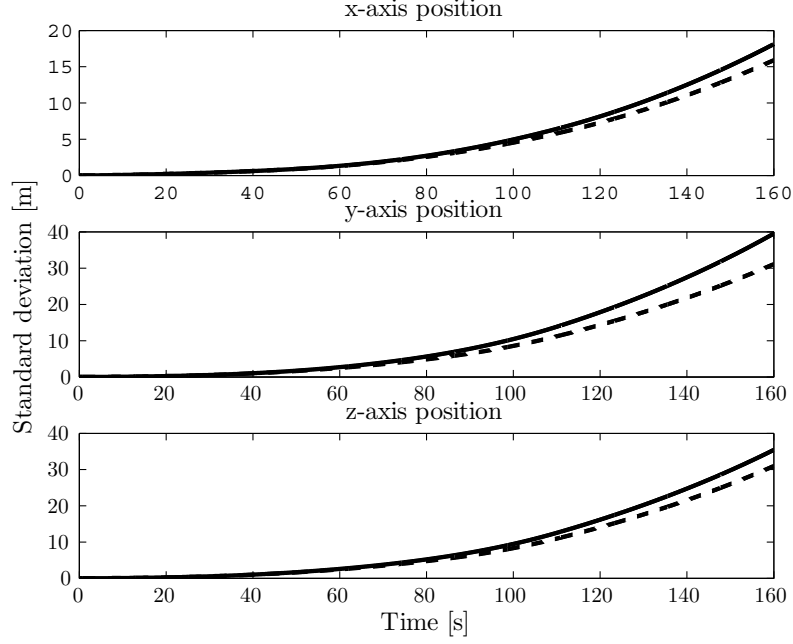
Figure 8: Position error standard deviations (without GPS). The solid line represents the baseline model and dashed line the augmented model.

Table 1: Precision improvement at the end of the endoatmospheric phase.

		w GPS	w/o GPS
	roll	68%	70%
Attitude	pitch	2%	6%
	yaw	27%	23%
	x	0%	12%
Velocity	y	12%	22%
	z	1%	11%
	x	0%	12%
Position	y	0%	21%
	z	0%	13%

For the robustness to modelling and parameters errors, the baseline model estimated standard deviations are compared to the estimated and real standard deviations of the augmented model. The real standard deviations of the baseline model are not presented, since they are accurately estimated and are not affected by the parameter and modelling errors considered here. Table 2 displays the results of the underestimated wind level when the GPS is present. Surprisingly, the real precision is, in many cases, better than the estimated one. This can be attributed to the tuning of the state covariance matrix of the Kalman filter, in which the variance of the state vector related to the augmented model is overestimated. Table 3 shows the results when the GPS is absent. In this case, some estimated standard deviations are optimistic, however the real standard deviations remain within the same range as with the baseline model. Either if the GPS is present or not, the roll and yaw estimations are significantly improved. This proves that even if some external perturbations are not considered or underestimated, the augmented model still performs well and would not compromise the mission.

11

Table 2: Error standard deviations at the end of the endoatmospheric phase with underestimated wind (with GPS).

| | | Baseline | Angmented | |
		Est.	Est.	Real
Attitude	roll	0.00028	0.00009	0.00004
[rad]	pitch	0.00008	0.00007	0.00007
	yaw	0.00008	0.00006	0.00005
Velocity	x	0.0091	0.0091	0.0084
[m/s]	y	0.0123	0.0109	0.0105
	z	0.0123	0.0122	0.0117
Position	x	0.068	0.068	0.078
[m]	y	0.070	0.070	0.070
	z	0.070	0.070	0.077

Table 3: Error standard deviations at the end of the endoatmospheric phase with underestimated wind (without GPS).

| | | Baseline | Angmented | |
		Est.	Est.	Real
Attitude	roll	0.00031	0.00009	0.00013
[rad]	pitch	0.00031	0.00029	0.00035
	yaw	0.00031	0.00023	0.00023
Velocity	x	0.20	0.18	0.25
[m/s]	y	0.70	0.54	0.62
	z	0.67	0.59	0.82
Position	x	18	16	22
[m]	y	39	31	38
	z	35	31	44

Table 4 shows the effect of a modelling error when the GPS is present. The roll estimation is still significantly improved, but the yaw estimation real standard deviation is doubled compared to the baseline model. The other results remain within the same range as with the baseline model. In table 5, the results without GPS are presented. The roll estimation is, again, greatly improved by the augmented model. However, the other estimations are similar to the ones obtained with the baseline model. The estimated standard deviations of the augmented model are slightly optimistic. These results indicate that the augmented model still performs well with modelling errors. However, the yaw estimation with GPS indicates that the augmented model could be sensitive to modelling errors on the launcher and control dynamics. Fortunately, this dynamics is usually well known which minimizes modelling errors. It highlights the fact that special care must be taken to avoid oversimplification of the model.

Table 4: Error standard deviations at the end of the endoatmospheric phase with angular dynamics modelling errors (with GPS).

		Baseline	Angmented	
		Est.	Est.	Real
Attitude	roll	0.00028	0.00016	0.00008
[rad]	pitch	0.00008	0.00008	0.00008
	yaw	0.00008	0.00006	0.00016
Velocity	x	0.0091	0.0091	0.0080
[m/s]	y	0.0123	0.0113	0.0149
	z	0.0123	0.0122	0.0119
Position	x	0.068	0.068	0.067
[m]	y	0.070	0.070	0.066
	z	0.070	0.070	0.068

Table 5: Error standard deviations at the end of the endoatmospheric phase with angular dynamics modelling errors (without GPS).

		Baseline	Angmented	
		Est.	Est.	Real
Attitude	roll	0.00031	0.00016	0.00017
[rad]	pitch	0.00031	0.00029	0.00030
	yaw	0.00031	0.00026	0.00027
Velocity	x	0.20	0.18	0.22
[m/s]	y	0.70	0.56	0.70
	z	0.67	0.60	0.70
Position	x	18	16	17
[m]	y	39	32	43
	z	35	31	36

6. CONCLUSION. In this paper, the reference trajectory is exploited to improve the performance of a navigation solution. It is shown that even when the navigation precision is good, this one can be improved without any additional sensors by the use of the reference trajectory data. The roll estimation benefits the most from the additional information, with a standard deviation reduced by 68%. Furthermore, the robustness to a GPS outage is greatly improved with a precision gain of at least 6% for all estimated values. Again, the roll is the one that gets the best improvement with 70%. The great improvement on the roll estimation is partly due to the weak observability of this value provided by the GPS. Considering that most of the external perturbations are concentrated into the endoatmospheric phase, the performance gain during the exoatmospheric phase is expected to be superior to the one obtained here. In view of the great results already obtained and the short duration of the complete mission (less than 12 minutes), it would be interesting to take the utilization of commercial grade sensors into consideration.

The robustness tests show that the augmented model can withstand great errors in the variances of the external perturbations. However, this one could be sensitive to modelling errors on the angular dynamics of the launcher and control. Fortunately, this dynamics is usually well known.

This paper presents the potential improvement provided by the uses of the reference trajectory data in the navigation solution. Further work is needed to get a more complete wind model. Also, the principle has to be validated on the complete launcher simulator. Finally, additional robustness tests are required.

REFERENCES

Ali, J. and Fang, J. (2009). Realization of an autonomous integrated suite of strapdown astro-inertial navigation systems using unscented particle filtering. *Computers & Mathematics with Applications*, 57(2):169–183.

Ali, J. and Jiancheng, F. (2006). Sins/ans integration for augmented performance navigation solution using unscented kalman filtering. *Aerospace Science and Technology*, 10(3):233–238.

Bancroft, J. B. (2009). Multiple imu integration for vehicular navigation. In *22nd International Technical Meeting of the Satellite Division of the Institute of Navigation 2009, ION GNSS 2009*, volume 2, pages 1026 – 1038, Savannah, GA, United states.

Barbour, N. M. (2011). Inertial navigation sensors. Technical Report RTO-EN-SET-116(2011), North Atlantic Treaty Organization.

Belin, S., Averlant, J.-F., Dubuc, F., Villers, S., and Reis, A. (2010). Requirements toward gnss chain for ariane 5 mid-life evolution. In *Proceedings 2010 5th ESA Workshop on Satellite Navigation Technologies & European Workshop on GNSS Signals and Signal Processing (NAVITEC 2010)*, pages 8 pp. –, Piscataway, NJ, USA.

Bletsos, N. A. (2004). Guidance, navigation, and control. http://www.aerospace.org/wp-content/uploads/crosslink/V5N1.pdf.

Brown, A. and Mathews, B. (2007). Constrained beamforming for space gps navigation. In *20th International Technical Meeting of the Satellite Division of The Institute of Navigation*, volume 2, pages 2357–2363, Fort Worth, TX, United states. ION.

de Castro Leite Filho, W. (2000). Control system of brazilian launcher. In *Proceedings 4th ESA International Conference on Spacecraft Guidance, Navigation and Control Systems and Tutorial on Modern and Robust Control: Theory, Tools and Applications (SP-425)*, pages 401–405, Noordwijk, Netherlands.

Duplain, . (2012). Contrôle d'un lanceur de satellite de petite taille. Master's thesis, Université Laval.

Ferguson, R. C. (2011). Evolution of the space shuttle primary avionics software and avionics for shuttle derived launch vehicles. In *SAE Technical Papers*, pages 923 – 933, Toulouse, France.

Giroux, R. (2004). *Capteurs bas de gamme et systèmes de navigation inertielle: nouveaux paradigmes d'application*. PhD thesis, École de technologie supérieure, département de génie électrique.

Goodman, J. L. and Propst, C. A. (2008). Operational use of gps navigation for space shuttle entry. In *Position Location and Navigation Symposium (PLANS)*, pages 731–743, Monterey, CA, United states. IEEE.

Gross, J., Gu, Y., Gururajan, S., Seanor, B., and Napolitano, M. R. (2010). A comparison of extended kalman filter, sigma-point kalman filter, and particle filter in gps/ins sensor fusion. In *Guidance, Navigation, and Control Conference*, number AIAA 2010-8332, Toronto, ON, Canada. AIAA.

Groves, P. D. and Long, D. C. (2005). Combating gnss interference with advanced inertial integration. *Journal of Navigation*, 58(3):419–432.

Hanson, J. M., Shrader, M. W., and Cruzen, C. A. (1995). Ascent guidance comparisons. *The Journal of the Astronautical Sciences*, 43(3):307–326.

Hao, Y. C., Ying, L., Xiong, K., Cheng, H. Y., and Qiao, G. D. (2010). Compact autonomous navigation system (cans). In *International Conference on Space Optics*.

Kachmar, P. M. and Wood, L. (1995). Space navigation applications. *Navigation*, 42(1):187–234.

Koelle, D. E. (2005). Cost efficiency as design and selection criterion for future launch vehicles. *Acta Astronautica*, 57:623 – 629.

Lu, P., Sun, H., and Tsai, B. (2003). Closed-loop endoatmospheric ascent guidance. *Journal of Guidance, Control and Dynamics*, 26(2):283–294.

Ma, W., Luo, J., Wang, M., and Yang, B. (2009). Performance discussion on space integrated navigation based three gps satellites. In *Proceedings of 9th International Conference on Electronic Measurement and Instruments (ICEMI)*, pages 3326–3329, Beijing, China.

Mori, H. (1999). Control system design of flexible-body launch vehicles. *Control Engineering Practice*, 7(9):1163 – 1175.

Ning, X. and Fang, J. (2008). Spacecraft autonomous navigation using unscented particle filter-based celestial/doppler information fusion. *Measurement Science & Technology*, 19(9):095203.

Samaan, M. and Theil, S. (À paraitre 2011). Development of a low cost star tracker for the shefex mission. *Aerospace Science and Technology*.

Savage, P. G. (2007). *Strapdown analytics*. Strapdown Associates, Inc.

Schmidt, G. T. (2010). Ins/gps technology trends. Technical Report RTO-EN-SET-116(2010), North Atlantic Treaty Organization.

Sedlak, J. E. (1997). Improved spacecraft attitude filter using a sequentially correlated magnetometer noise model. In *Digital Avionics Systems Conference*, volume 2, pages 8.4–9–8.4–16, Irvine, CA, USA. AIAA/IEEE.

Tanenhaus, M., Geis, T., Carhoun, D., and Holland, A. (2010). Accurate real time inertial navigation device by application and processing of arrays of mems inertial sensors. In *Position Location and Navigation Symposium (PLANS)*, pages 20–26, Palm Springs, CA, USA. IEEE/ION.

Theil, S., Schlotterer, M., Hallmann, M., and Conradt, M. (2008). Hybrid navigation system for the shefex-2 mission. In *Guidance, Navigation and Control Conference and Exhibit*, number AIAA 2008-6991, Honolulu, HI, USA. AIAA.

Theil, S., Steffes, S., Samaan, M., Conradt, M., Markgraf, M., and Vanschoenbeek, I. (2009). Hybrid navigation system for spaceplanes, launch and re-entry vehicles. In *16th International Space Planes and Hypersonic Systems and Technologies Conference*, number AIAA 2009-7381, Bremen, Germany. AIAA/DLR/DGLR.

Titterton, D. H. and Weston, J. L. (2004). *Strapdown inertial navigation technology-2nd edition*. The Institution of Electrical Engineers, Stevenage, UK.

Vachon, A. (2012). *Trajectographie d'un lanceur de satellites basée sur la commande prédictive*. PhD thesis, Université Laval, département de génie électrique et génie informatique.

Vachon, A., Gagnon, E., R., F., and Desbiens, A. (2010). Équations de la dynamique de translation d'un lanceur. Technical report, R&D pour la Défense Canada - Valcartier.

Waldmann, J. (2007). Feedforward ins aiding: an investigation of maneuvers for in-flight alignment. *Controle y Automacao*, 18(4):459–470.

Wang, L., Ye, P., Zhai, C., and Y., Z. (2008). High performance strapdown inertial navigation system algorithms for space flight. In *2nd International Symposium on Systems and Control in Aerospace and Astronautics (ISSCAA)*, pages 1–5, Piscataway, NJ, USA.

Woodman, O. J. (2007). An introduction to inertial navigation. Technical Report UCAM-CL-TR-696, University of Cambridge, computer laboratory.

Yu, L., Chen, S., Ouyang, J., Zuo, C., Chen, X., Wu, S., and Yang, X. (2010). Error compensation and implementation of embedded high-precision magnetometer. In *International Conference on Electrical and Control Engineering (ICECE)*, pages 911–914, Wuhan, China.

Yuksel, Y., El-Sheimy, N., and Noureldin, A. (2010). Error modeling and characterization of environmental effects for low cost inertial mems units. In *Position Location and Navigation Symposium (PLANS)*, pages 598–612, Palm Springs, CA, USA. IEEE/ION.

Zhang, H., Zheng, W., and Tang, G. (À paraitre 2011). Stellar/inertial integrated guidance for responsive launch vehicles. *Aerospace Science and Technology*.

APPENDIX

A. LOOSELY COUPLED NAVIGATION EQUATIONS. This section presents the matrices and error state vector used for the loosely coupled part of the equations (12) and (13). The error state vector is:

$$x_{lc}^E = \begin{bmatrix} \delta\Psi_e^E \\ \delta v_e^E \\ \delta r_e^E \end{bmatrix} \tag{A1}$$

where $\delta\Psi$ is the attitude error represented in the Earth frame.

The state evolution matrix is:

$$A1 = \begin{bmatrix} -[\omega_r]_{IE}^E \times & 0_{3\times3} & 0_{3\times3} \\ [\mathbf{T_e}]_{\mathbf{B}}^{\mathbf{E}} a_m^B \times & -2[\omega_r]_{IE}^E \times & 0_{3\times3} \\ 0_{3\times3} & I_3 & 0_{3\times3} \end{bmatrix} \tag{A2}$$

where $[\omega_r]_{IE}^E \times$ is the skew symmetric matrix of the angular speed of the Earth rotation and $a_m^E \times$ is the skew symmetric matrix of the measured acceleration both represented in the Earth frame. $0_{i\times j}$ is a $i \times j$ zeros matrix and I_i is a $i \times i$ identity matrix.

The input matrix is:

$$\begin{bmatrix} B1 & B2 \end{bmatrix} = \begin{bmatrix} -[\mathbf{T_e}]_{\mathbf{B}}^{\mathbf{E}} & 0_{3\times3} \\ 0_{3\times3} & [\mathbf{T_e}]_{\mathbf{B}}^{\mathbf{E}} \\ 0_{3\times3} & 0_{3\times3} \end{bmatrix} \tag{A3}$$

where $[\mathbf{T_e}]_{\mathbf{B}}^{\mathbf{E}}$ is the rotation matrix from the body frame to the Earth frame.

The observation matrix is:

$$\begin{bmatrix} C1 \\ C2 \end{bmatrix} = \begin{bmatrix} 0_{3\times3} & I_3 & 0_{3\times3} \\ 0_{3\times3} & 0_{3\times3} & I_3 \end{bmatrix} \tag{A4}$$

B. AUGMENTED MODEL EQUATION. This section presents the matrices and vector which were employed for the augmented part in the equations (12) and (13). They are used to propagate the divergence between the launcher and reference attitude.

The augmented vector is:

$$x_a^B = \begin{bmatrix} x_{10} \\ x_{11} \\ x_{12} \\ x_{13} \\ x_{14} \\ x_{15} \\ x_{16} \\ \delta\Psi_{ref}^B \end{bmatrix} \tag{B1}$$

where $x_{10}, x_{11}, x_{12}, x_{13}, x_{14}, x_{15}$ and x_{16} are intermediate states used to calculated the dynamics of the propagation and $\delta\Psi_{ref}$ is the divergence between the launcher and reference attitude.

The propagation of the navigation error into the augmented model is:

$$A2 = \begin{bmatrix} \begin{bmatrix} [\mathbf{T_e}]_{\mathbf{E}}^{\mathbf{B}} & 0_{3\times3} & 0_{3\times3} \end{bmatrix} \\ 0_{7\times9} \end{bmatrix} \tag{B2}$$

where $[\mathbf{T_e}]_{\mathbf{E}}^{\mathbf{B}}$ is the estimated rotation matrix from the Earth frame to the body frame.

Combining the equation (8) and the corresponding dynamics equation for each angle (equations (14), (15) and (16)), gives the complete dynamics of the divergence propagation between

the launcher and reference attitude. This one is represented by:

$$A3 = \begin{bmatrix} \begin{bmatrix} -0.5 & 0 & 0 \\ 0 & -6.1248 & 0 \\ 0 & 0 & -6.1248 \end{bmatrix} & \begin{bmatrix} 0 & 0 \\ 5.6922 & 0 \\ 0 & 5.6922 \end{bmatrix} & 0_{3\times2} & -I_3 \\ \begin{bmatrix} 0 & 1 & 0 \\ 0 & 0 & 1 \end{bmatrix} & 0_{2\times2} & 0_{2\times2} & 0_{2\times3} \\ 0_{2\times3} & I_2 & 0_{2\times2} & 0_{2\times3} \\ \begin{bmatrix} 0.6 & 0 & 0 \\ 0 & 30.012 & 0 \\ 0 & 0 & 30.012 \end{bmatrix} & \begin{bmatrix} 0 & 0 \\ 10.7475 & 0 \\ 0 & 10.7475 \end{bmatrix} & \begin{bmatrix} 0 & 0 \\ 0.8111 & 0 \\ 0 & 0.8111 \end{bmatrix} & 0_{3\times3} \end{bmatrix} \tag{B3}$$

The input matrix is:

$$B3 = \begin{bmatrix} 0_{7\times3} \\ I_3 \end{bmatrix} \tag{B4}$$

The observation matrix is:

$$\begin{bmatrix} C3 & C4 \end{bmatrix} = \begin{bmatrix} I_3 & 0_{3\times6} & 0_{3\times7} & [\mathbf{T_e}]_\mathbf{B}^\mathbf{E} \end{bmatrix} \tag{B5}$$